

Skeleton-geodesic Distances for Shape Recognition: Efficient Computation by Continuous Skeleton

Nikita Lomov

Lomonosov Moscow State University, GSP-1, Leninskie Gory, Moscow, 119991, Russian Federation

Keywords: Shape Description, Skeleton-geodesic Distance, Shape Context, Polygonal Figure, Voronoi Diagram.

Abstract: We consider the problem of determining the distance between points of a planar shape, which would be informative and resistant to shape transformations, including flexible articulations. The proposed distance is defined as the length of the shortest path through the skeleton between the projections of the points on the skeleton and called skeleton-geodesic distance. To calculate the values of interest, a continuous medial representation of polygonal shape is used. The method of calculating the distance is based on the following principle: at first, calculate all skeleton-geodesic distances between pairs of “reference” points, which are the vertices of the skeleton, using the traditional graph algorithms; then refine them by adding the distances from the points in question to the nearest reference points. This approach allows us to achieve computational efficiency and to derive analytical formulas for direct calculation. An analogue of shape context using skeleton-geodesic distances and angles between branches of the skeleton is proposed. Examples of using these descriptors in the task of recognition of flexible objects are presented, showing that the distance proposed often provides greater performance compared to Euclidean or geodesic distances.

1 INTRODUCTION

In computer vision tasks related to the shape recognition for objects in images, methods that use the distribution of distances between points of the shape in a feature description are very popular. Perhaps the most famous of these methods is the shape context (Belongie et al., 2002), which builds joint histograms of distances and angles for contour points. However, it was noted that the Euclidean distance used in this method does not describe shapes very well in the case of flexible articulations. Therefore, modifications of this algorithm were developed, using the distance of path lying inside the figure (Ling and Jacobs, 2007), otherwise — geodesic distances (Jain and Zhang, 2005). Geodesic distances are well established in the field of recognition of three-dimensional shapes (Shamai and Kimmel, 2017), where they also proved to be resistant to shape variations.

Existing algorithms of geodesic distances computation involve numerical methods like fast marching (Sethian, 1999) or other propagation techniques (Cárdenes et al., 2010) that operate on pixel level. This is time consuming, especially in cases when the distances between multiple points are analyzed, since it is necessary to run a geodesic distance transform for each of them. At the same time, there are examples

of distances, which are also determined by the lengths of the inner-paths of the figure, and therefore resistant to flexible deformations, but these paths are defined in a nontrivial way. Such an approach was proposed in (Cuisenaire, 1999), where the paths that lie inside the figure, but are sufficiently far from its border, were considered. In addition, in the paper (Boluk and Demirci, 2015) the distances from the points of the skeleton to the ends of its branches computed as the lengths of skeleton lines were investigated. Developing these ideas, in this paper we suggest an alternative of traditional geodesic distances — skeleton-geodesic distances, which are determined by the shortest paths lying on the medial axis. Skeleton-geodesic distances share many useful features of classic geodesic distances, such as rotation invariance and resistance to flexible articulations. At the same time their calculation uses a contour-skeleton representation, which is much more compact than pixel-wise. Moreover, it is sufficient to calculate the distances for a certain set of “reference” points, and the distances at intermediate points can be interpolated without loss of accuracy.

In Figure 1 you can see how much skeleton-geodesic distances differ from the usual ways of defining the distances between points of the shape.

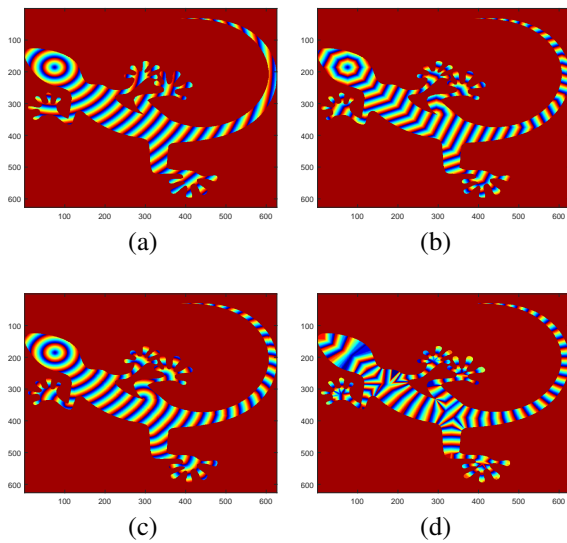


Figure 1: Map of distances to the same point for different types of distance: (a) Euclidean, (b) geodesic with quasi-Euclidean metric (c) geodesic with Euclidean metric, (d) skeleton-geodesic.

2 BASIC CONCEPTS

Definition 1. *Skeleton* is the set of centers of all inscribed empty (maximal by inclusion) circles of a shape.

Definition 2. *Skeleton-geodesic distance* between points p and q of the skeleton of figure A (denoted by $d_{Geod(Sk(A))}(p, q)$) is the length of the shortest path between these points passing through the skeleton¹.

Definition 3. *Spoke* is a line segment from the skeleton point to any nearest boundary point.

Definition 4. *Skeletal projection* of the point $p \in A$ (denoted by $p_{Sk(A)}$) is the origin of the spoke, which the point p lies on.

Since a set of spokes covers the entire figure, and for each of its points, the spoke is uniquely defined (Mestetskiy, 2015) the skeletal projection is also uniquely defined for each point of the shape. As a result, we can extend the definition 2 and calculate skeleton-based distances for all points of the figure.

Definition 5. *Skeleton-geodesic distance* between arbitrary points p and q of A is considered to be the skeleton-geodesic distance between their projections:

$$d_{Geod(Sk(A))}(p, q) = d_{Geod(Sk(A))}(p_{Sk(A)}, q_{Sk(A)}). \quad (1)$$

Note that the skeletal geodesic distance is not a distance in the strict sense, but is a factor-distance, since the distance between all points lying on the spokes with the same origin is equal to zero. Because

¹Further we use a simpler notation: $d_{skel}(p, q)$.

of this, we can talk about the distances between the spokes, as well as about the distances between individual points.

Methods for constructing continuous skeletons of polygonal figures, as well as for approximating objects in a binary image by polygons, are known and well developed (Mestetskiy and Semenov, 2008). The boundary of the polygonal figure can be represented as the set of point-sites (vertices of a figure) and segment-sites (sides of boundary polygons). Voronoi diagram (VD) of line segments is defined for these set of sites. The skeleton is obtained from the subgraph of VD lying inside the figure by cutting off the bisectors between concave point-sites and adjacent segment-sites. Each edge of the skeleton is associated with a pair of sites for which this edge is a bisector — the common boundary of their Voronoi cells. So, a skeleton of polygonal figure can be considered as a planar graph $S = (V, E)$ with edges in the form of linear and parabolic segments.

Definition 6. *Bicircle* of the edge $e \in E$ is the union of all inscribed circles centered on e . The edge is called the axis of bicircle.

Definition 7. *Proper region* of the bicircle of edge e is the closure of the union of all spokes incidental to internal points of e .

Proper regions cover the entire figure and intersect only along their boundary spokes. These concepts will help us in the direct calculation of skeleton-geodesic distances.

3 IDEA OF THE ALGORITHM

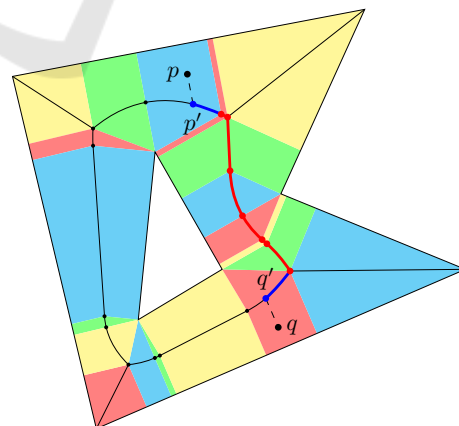


Figure 2: Example of skeleton-geodesic path between points p and q lying on the spokes $p'p''$ and $q'q''$ respectively. It consists of the main part located between the vertices of the skeleton (red line) and additions — parts lying inside proper regions of p and q (blue lines). Proper regions are painted in different colors.

The skeleton-geodesic distance between the points p and q can be calculated once as follows:

1. Find the skeletal projections of p and q .
2. For projections that do not coincide with the vertices of the skeleton, split the edges to which they belong into two parts.
3. Use the standard shortest-path search algorithm in the graph for a modified (with edges split) skeleton — Dijkstra's algorithm or one of the algorithms for determining the least common ancestor if there are no cycles in the skeleton and it can be represented by a tree.

This approach is illustrated in Figure 2. Nevertheless, it can be ineffective in a mass query, as it will require constant modification of the original graph and repeated launch of the shortest path algorithm for very similar graphs.

Notice that to determine the skeletal projection of an arbitrary point of a figure, we can first determine its proper region. The desired region can be found as a result of solving the geometric search problem, or, which is a more realistic option, — in the case of uniform generation of points inside the figure or on the contour, the necessary points can be generated for each proper region separately.

Suppose the skeleton is structured so that for any adjacent vertices, the shortest path along the skeleton is the edge connecting them. Consider the point p_1 belonging to the proper region of the edge (a_1, b_1) of length l_1 , and the point p_2 belonging to the proper region of the edge (a_2, b_2) of length l_2 . Let also $d_{skel}(p_1, a_1) = d_1$ and $d_{skel}(p_2, a_2) = d_2$. Then

$$\begin{aligned} d_{skel}(p_1, b_1) &= l_1 - d_1, \\ d_{skel}(p_2, b_2) &= l_2 - d_2. \end{aligned} \quad (2)$$

In this case, two different options can be distinguished:

1. The edges (a_1, b_1) and (a_2, b_2) are the same. Then

$$d_{skel}(p_1, p_2) = |d_1 - d_2|. \quad (3)$$

2. The edges (a_1, b_1) and (a_2, b_2) are different. Then

$$\begin{aligned} d_{skel}(p_1, p_2) &= \min(d_{skel}(a_1, b_1) + d_1 + d_2, \\ & d_{skel}(a_1, b_2) + d_1 + l_2 - d_2, \\ & d_{skel}(a_2, b_1) + l_1 - d_1 + d_2, \\ & d_{skel}(a_2, b_2) + l_1 - d_1 + l_2 - d_2). \end{aligned} \quad (4)$$

Bicircle is called monotonic, if the radial function (the radius of inscribed circle) decreases or increases monotonically along its axis. It can be shown that the path between the points of the same edge does not go beyond it if all bicircles of the skeleton are monotonic. Thus, it is more convenient to consider only monotonic bicircles. As shown in (Lomov and Mestetskii,

2017), a nonmonotonic bicircle can always be split into a pair of monotonic ones with the disjointness property of proper regions preserved.

In this case, in turn, two new questions arise: how to determine $d_{skel}(u, v)$ for the ends of the edges $u, v \in V$ and how to determine $d_i, i = 1, 2$. The first problem is solved by running the Johnson algorithm (Johnson, 1977) to search for all shortest paths in a skeleton graph. The progress of the second one depends on the type of proper region, the coordinates of its points and the coordinates of the point p itself. Consider the regions of each type in more detail.

4 SEARCH FOR THE INCIDENT SPOKE

Three types of bicircles are distinguished depending on the pair of generating sites of its edge: linear (two segment-sites), parabolic (segment-site and point-site) and hyperbolic (two points-sites). Such terminology is motivated by the nature of the dependence of inscribed circle radius on the position of the point on the axis of the bicircle. The axis of the parabolic bicircle is a segment of the parabola, and axes of other two types are linear segments. Further we denote the ends of the edge of the bicircle as A and B , an arbitrary point of the proper region as P , the length of the edge as l and $d_{skel}(P, A) = \lambda$.

4.1 Linear Bicircle

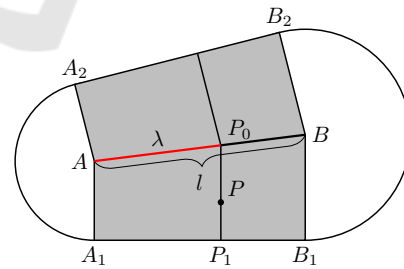


Figure 3: Linear bicircle.

Let the projections of A and B onto the first site are A_1 and B_1 and onto the second site are A_2 and B_2 respectively (Figure 3). Without loss of generality, we assume that P is closer to the site A_1B_1 , i.e. belongs to the polygon AA_1B_1B . Let P belong to the spoke P_0P_1 , $P_0 \in AB$, $P_1 \in A_1B_1$. Then $P_0P \parallel AA_1$, which means

$$(x_{P_0}, y_{P_0}) = (x_A + \alpha(x_B - x_A), y_A + \alpha(y_B - y_A)),$$

$$\frac{x_P - x_A - \alpha(x_B - x_A)}{x_{A_1} - x_A} = \frac{y_P - y_A - \alpha(y_B - y_A)}{y_{A_1} - y_A}, \quad (5)$$

$$\alpha = \frac{(x_P - x_A)(y_{A_1} - y_A) - (y_P - y_A)(x_{A_1} - x_A)}{(y_B - y_A)(x_{A_1} - x_A) - (x_B - x_A)(y_{A_1} - y_A)},$$

and $\lambda = \alpha l$.

4.2 Hyperbolic Bicircle

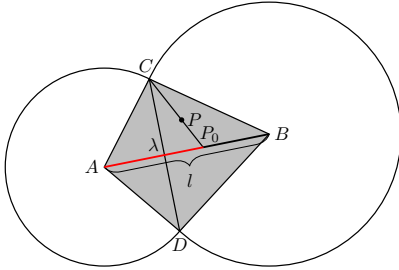


Figure 4: Hyperbolic bicircle.

Denote the point-sites C and D and suppose that P is closer to the site C , that is, it is located inside triangle ACB (Figure 4). If P coincides with C , then a continuum of spokes passes through this point. Although the set of such “singular” points has measure zero, in this case the required spoke by definition is the one with the minimum length (since a site-point can lie on the border of several proper regions, the desired spoke can be located in another region).

If $P \neq C$, a unique spoke passes through P , starting from the point $P_0(x_A + \alpha(x_B - x_A), y_A + \alpha(y_B - y_A))$. Find α . According to the equation of the line,

$$\frac{x_P - x_C}{x_A + \alpha(x_B - x_A) - x_C} = \frac{y_P - y_C}{y_A + \alpha(y_B - y_A) - y_C},$$

$$(x_P - x_C)(y_A + \alpha(y_B - y_A) - y_C) = (y_P - y_C)(x_A + \alpha(x_B - x_A) - x_C), \quad (6)$$

$$\alpha = \frac{(y_P - y_C)(x_A - x_C) - (x_P - x_C)(y_A - y_C)}{(x_P - x_C)(y_B - y_A) - (y_P - y_C)(x_B - x_A)},$$

and $\lambda = \alpha l$.

4.3 Parabolic Bicircle

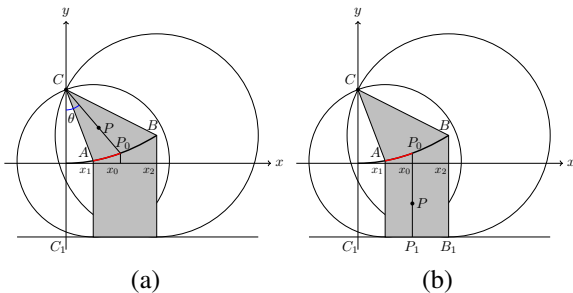


Figure 5: Parabolic bicircle.

The case of a parabolic bicircle is the most complicated. Firstly, the length of the parabolic edge is not equal to the Euclidean distance between its ends, but is calculated by the formula

$$L(x_1, x_2) = \frac{x_2 \sqrt{x_2^2 + p^2} - x_1 \sqrt{x_1^2 + p^2}}{2p} + \frac{p}{2} \ln \left| \frac{x_2 + \sqrt{x_2^2 + p^2}}{x_1 + \sqrt{x_1^2 + p^2}} \right|, \quad (7)$$

where $x_1 = \sqrt{2p(|AC| - \frac{p}{2})}$, $x_2 = \sqrt{2p(|BC| - \frac{p}{2})}$ and p is the focal parameter of the parabola. First, consider the case in which the nearest site is a point-site (Figure 5a). Denote C_1 the projection of the point-site on the segment-site, then $p = |CC_1|$. Let the angle C_1CP be equal to θ , then, according to the equation of the parabola in the polar coordinate system, the radial function in the origin of the desired spoke P_0 is equal to $\rho = \frac{p}{1 + \cos\theta}$, and its abscissa is equal to $x_0 = \sqrt{2p(\rho - \frac{p}{2})}$.

If the closest site is a segment-site, we determine the value x_0 as $|C_1P_1|$ (Figure 5b):

$$x_0 = \frac{\langle \vec{C_1P}, \vec{C_1B_1} \rangle}{x_2}. \quad (8)$$

Then, regardless of which site is the closest, λ is calculated by the formula

$$\lambda = L(x_1, x_0). \quad (9)$$

5 SKELETON-GEODESIC SHAPE CONTEXT

The classic shape context introduced in (Belongie et al., 2002) analyzes the relative position of the contour points $\{p_j\}$ relative to the selected point p_i using the Euclidean distance r and polar angle ϕ :

$$h_i(k, t) = \#\{p_j : j \neq i, \quad r(p_j - p_i) \in \text{bin}_r(k), \quad \phi(p_j - p_i) \in \text{bin}_\phi(t)\} \quad (10)$$

In that case, if the shape is subjected to flexible articulations, say, the rotation of individual shape parts around their junctions, such distances are unstable. In (Ling and Jacobs, 2007) an alternative approach to determining distances and angles in calculating the shape context was proposed. The distance is the length of the shortest path between the points lying entirely inside the figure, i.e. geodesic distance (the term *inner-distance* is used in the article). Since the contour representation is used in the form of closed polylines, the shortest path from P to Q is also a polygonal chain. We denote its vertices by $C_1C_2 \dots C_N$, $C_1 = P$, $C_N = Q$. The *inner-angle* when calculating the descriptor for P is the angle between the tangent to the contour in P and the vector

$\overrightarrow{C_1 C_2}$. Such an angle is not only insensitive to rotation, but also to articulations of individual parts of the shape, since they lead to bendings in the middle sections of the shortest path, and the direction of its beginning in the local coordinate system associated with the boundary tangent changes slightly.

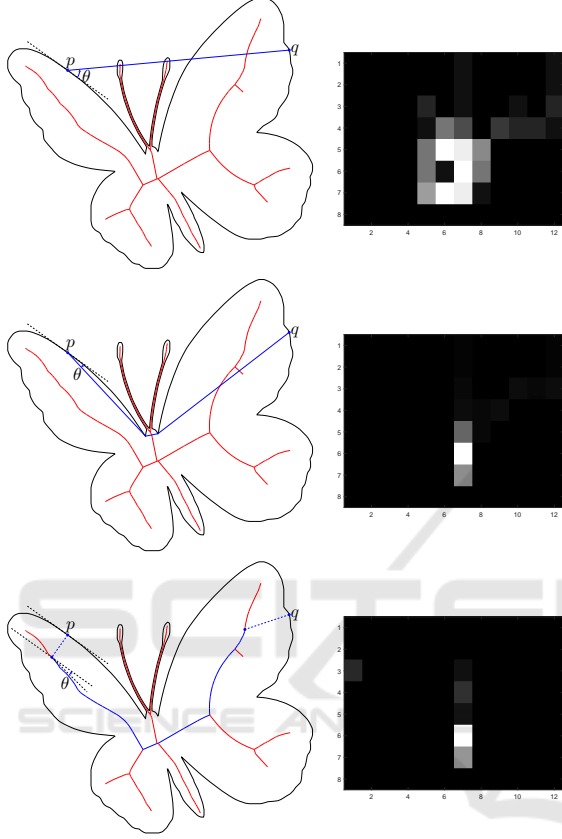


Figure 6: Shape context of different types calculated for p : Euclidean (top row), geodesic (middle), skeleton-geodesic (bottom). The shortest path from p to q is shown in blue.

Developing these ideas, we suggest a new variation of shape context, *skeleton-geodesic shape context*. The distance is considered to be skeleton-geodesic distance, and the angle is the angle between the tangent to the skeleton edge at the start of the shortest path and the tangent to the boundary. The skeleton-geodesic shape context shares necessary insensitivity properties to rotations and articulations with the inner-distance shape context.

The types of defining the shape context are shown in Figure 6. In contrast to the Euclidean distance shape context, inner-distance and skeleton-geodesic distance contexts lead to a much more concentrated distribution of characteristics in the feature space.

For shape matching and comparison we will use the dynamic programming approach proposed in

(Ling and Jacobs, 2007). Given two shapes A and B described by point sequences on their contour, e.g., p_1, p_2, \dots, p_n for A with n points, and q_1, q_2, \dots, q_m for B with m points. The matching from A to B is a mapping from $1, 2, \dots, n$ to $0, 1, 2, \dots, m$, where p_i is matched to $q_{\pi(i)}$ if $\pi(i) \neq 0$ and otherwise left unmatched. π should minimize the match cost $C(\pi)$ defined as

$$C(\pi) = \sum_{1 \leq i \leq n} c(i, \pi(i)) \quad (11)$$

where $c(i, 0) = \tau$ is the penalty for leaving p_i unmatched, and for $1 \leq j \leq m$, $c(i, j)$ is the cost of matching p_i to q_j . For example, the distance between two K -bin shape context histograms $h_{A,i}$ and $h_{B,j}$ of points $p_i \in A$ and $q_j \in B$ respectively is defined using the χ_2 statistic:

$$c(i, j) \equiv \frac{1}{2} \sum_{1 \leq k \leq K} \frac{[h_{A,i}(k) - h_{B,j}(k)]^2}{h_{A,i}(k) + h_{B,j}(k)}. \quad (12)$$

The skeleton-geodesic shape context of p_i can be calculated directly, assuming that the points of interest are distributed uniformly along the contour C , by analyzing the distribution function

$$\begin{aligned} F_{R, \Phi}(a, b) &= \mathbb{P}(R \leq a, \Phi \leq b) \\ &= \mathbb{P}(r(p - p_i) \leq a, \phi(p - p_i) \leq b \mid p \sim U(C)), \end{aligned} \quad (13)$$

$$\frac{h_i(k, t)}{n-1} \approx \mathbb{F}_{R, \Phi}(a_k, b_t) - \mathbb{F}_{R, \Phi}(a_{k-1}, b_{t-1}), \quad (14)$$

where $[a_{k-1}, a_k]$ and $[b_{t-1}, b_t]$ are the bounds of the k -th and t -th histogram bins for distance and angle.

Breaking the contour into disjoint sections coinciding with the boundaries of the bicircles, we can consider each edge individually and reconstruct the result using the Bayes' formula.




6 EXPERIMENTS

6.1 Runtime Analysis

Proposed algorithm for calculating skeleton-geodesic distances (SGD) implemented in C++ was compared in terms of time-consumption with algorithm of geodesic distance transform (GDT) computation from (Cárdenes et al., 2003), because its source code is available for free. To compare a similar output format, distance transforms — maps of the distances from the selected point to points with integer coordinates — were calculated. Time was averaged over 10000 launches of DT. The experiments were conducted on a laptop with Intel®Core™i5-4210U and 6GB RAM.

Results (Table 1) show that the proposed algorithm requires appreciable time for preprocessing, but after it works significantly faster than its counterpart. It is also confirmed that the preprocessing time depends on the complexity of the skeleton representation, whereas the time of distance map computation is linear in the number of pixels. Analytical calculation of the shape context context (SC) pays off if the number of edges of the skeleton is much lower than n , the number of points sampled at the contour. Since n usually does not exceed several hundred, this approach is justified only for fairly simple shapes.

Table 1: Computational costs for the construction of geodesic distance descriptors.

Image			
Size	626 × 562	322 × 512	2000 × 1053
Object pixels	73214	53531	297438
Skeleton edges	910	2672	8729
GDT time, ms	22.412	13.353	91.712
SGDT time, ms	2.279	1.815	10.547
SGD preproc. time, ms	76	958	9935
SC time (1 point), ms	0.310	0.624	1.975

6.2 Recognition by Histograms

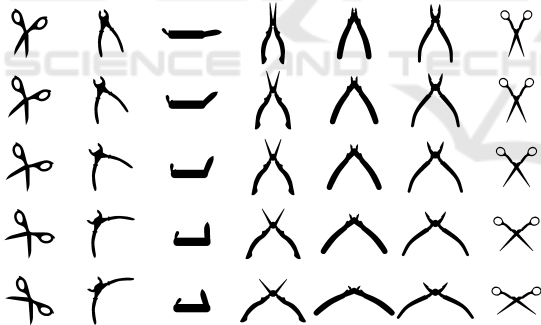


Figure 7: Images from Tools dataset.

Tools dataset (Bronstein et al., 2008) shown in Figure 7 consists of 35 images of articulated shapes (silhouettes): 5 images for 7 types of tools (scissors, pliers, pincers, knives). Each shape differs by an articulation. For every image cumulative skeleton-geodesic histogram, reflecting the proportion of pairs of points, the distance between which does not exceed a specified value, was computed. These histograms were normalized by the square of the area of the figure along the y-axis, and by the maximum distance in the figure along the x-axis. Thus, all histograms are located in a unit square. For greater visibility, the function of the basic profile, describing the distances be-

tween points from unit distribution on a line:

$$f(x) = 2x - x^2, \quad (15)$$

was subtracted. Thus, the increase of the resulting functions (Fig. 8) indicates the total concentration of points at a given distance level, and the decrease indicates the total rarefaction.

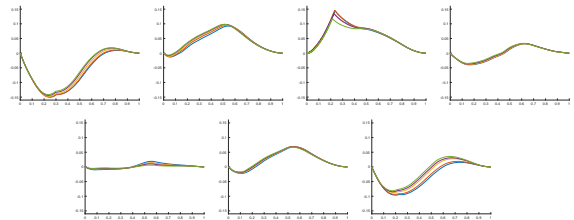


Figure 8: Skeleton-geodesic distance distributions for objects in Tools dataset. Each plot corresponds to one of seven classes.

After that, the L_1 -distances between the histograms were calculated, they are visualized in Figure 9a. For all 35 objects, the nearest 3 objects belong to the same class, and for only one object out of 35 the fourth nearest object belongs to the wrong class. At the same time, for geodesic distances, only 80% of the objects of the four nearest neighbors belong to the correct class (Fig. 9b). The experiment shows that the skeleton-geodesic distances are more resistant to the “hinge-type” articulations than usual geodesic ones. This can be explained by the fact that the skeleton, being equidistant from two contour sections, halves the deviation of one of them, if the second remains unchanged.

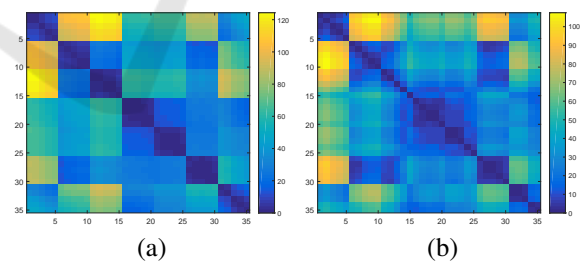


Figure 9: Dissimilarities between histograms of (a) skeleton-geodesic distances and (b) traditional geodesic distances for Tools dataset.

6.3 Recognition by Shape Context

Following experiments compare three types of shape context descriptors based on Euclidean distance, inner-distance and skeleton-geodesic distance. In all of them, the measure of difference between shapes will be calculated based on dynamic programming approach described above. Parameters

of the methods are n (number of contour points), n_d (number of distance bins in shape context histogram), n_θ (number of angle bins), k (number of points in primary alignment in DP method) and h (maximum Hausdorff distance between initial figure and figure after skeleton pruning). When conducting experiments, we used the code of Euclidean and inner-distance shape context available at http://www.dabi.temple.edu/~hbbling/code_data.htm (“Shape Matching” section).

6.3.1 Kimia 216 Dataset

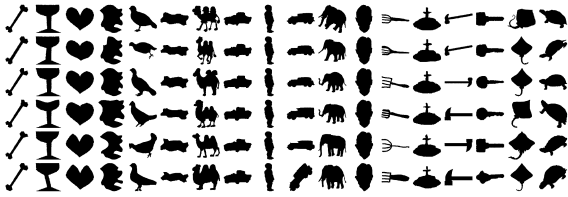


Figure 10: Half of the images from Kimia 216 dataset.

The Kimia 216 database² provided by Brown University contains 216 images from 12 categories (Fig. 10). We use parameters $n = 100$, $n_d = 5$, $n_\theta = 12$, $k = 4$ and $h = 1$. The retrieval result is summarized as the number of 1st, 2nd and 3rd closest matches that fall into the correct category. The results are listed in Table 2. It shows that skeleton-geodesic shape context determines the total population of images of the same class slightly better than its counterparts.

Table 2: Evaluation performance on Kimia 216 dataset.

Distance	1st	2nd	3rd	4th	5th	6th
Euclidean	216	216	215	215	213	213
Inner	216	216	215	214	213	211
Skeleton	216	216	215	214	214	212
Distance	7th	8th	9th	10th	11th	Total
Euclidean	211	204	201	193	184	96.00%
Inner	211	204	204	203	183	96.38%
Skeleton	211	208	208	206	189	97.18%

6.3.2 Swedish Leaf Dataset



Figure 11: Class instances from Swedish Leaf dataset.

The Swedish Leaf³ dataset provided by Linköping University contains isolated leaves from 15 different Swedish tree species, with 75 leaves per species

²<http://vision.lems.brown.edu/sites/default/files/216db.tar.gz>

³<https://www.cvl.isy.liu.se/en/research/datasets/swedish-leaf/>

(Fig. 11). We tested our descriptors with parameters $n = 128$, $n_d = 8$, $n_\theta = 12$, $k = 1$ (images are normalized by orientation, so we can assume that the top-left points should coincide) and $h = 2$. To evaluate the effect of choosing the type of distance, experiments with distance only ($n_\theta = 1$) were also conducted. We used a binarized version of this dataset and chose for each species 25 images for training and 50 for testing. Classification was done by nearest neighbor method, the recognition results are summarized in Table 3. It is noteworthy that adding information about the angles does not have a significant impact on the result, perhaps because of the convexity of most shapes. The good results of the Euclidean distance, apparently, are due to the fact that the shapes can be considered rigid, and not subject to significant articulations.

Table 3: Classification performance on Swedish Leaf dataset.

Distance type	Distance + angle	Distance only
Euclidean	94.80	94.00
Inner	94.13	92.80
Skeleton	94.67	93.20

6.3.3 MPEG7 Dataset

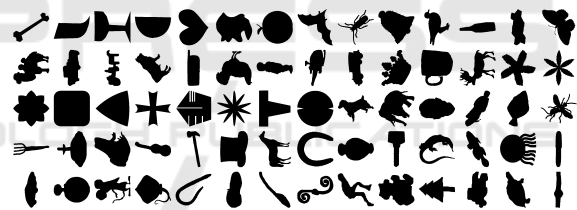


Figure 12: Class instances from MPEG7 dataset.

The widely tested MPEG7 CE-Shape-1⁴ database consists of 1400 silhouette images from 70 classes. Each class has 20 different shapes, first of them are shown in Fig. 12. The recognition rate is measured by the so-called Bullseye test: for every image in the database, the top 40 most similar candidates are determined and the percentage of hits in the top-40 of the desired class from the maximum possible (20×1400) is calculated. The parameters in our experiment are: $n = 100$, $n_d = 8$, $n_\theta = 12$, $k = 8$ and $h = 3$. When aligning the contours, the points were considered both in the forward and in the reverse order, to provide the resistance to reflection. Table 4 lists obtained results for different types of shape context taking into account angle information and without it.

Although our method is superior to its competitors with full information used, its advantage when work-

⁴<http://www.dabi.temple.edu/~shape/MPEG7/dataset.html>

Table 4: Classification performance on MPEG7 dataset.

Distance type	Distance + angle	Distance only
Euclidean	86.14	73.13
Inner	85.52	72.61
Skeleton	87.35	77.25

ing only with distances is much more impressive. This leaves open the question of a better determination of the angles between the points of the shape. In addition, histogram comparisons based on the χ^2 criterion are also not well suited for fairly concentrated distribution, such as skeleton-geodesic shape context, that leaves the task of designing a better way to compare such histograms for future research. We also note that, as in the previous experiment, the inner-distances did not demonstrate their advantage over the Euclidean ones, being used in completely the same manipulations.

7 CONCLUSION

In this article we proposed a method for describing the shape using the distribution of distances between its points, which are calculated using a skeleton. It is shown that using a continuous skeletal representation, the basis of calculations can be reduced to classical algorithms on graphs. Proposed distance can be used in many 2D shape recognition algorithms as a replacement for the Euclidean or geodesic distance, for example, we designed an analogue of very popular shape context descriptor. Remarkable that such descriptor can be considered from the point of view of probability theory, it can be calculated with high accuracy based on the continuous model, and all the necessary formulas are derived analytically. Estimates of temporal costs show that the method takes some time to preprocess the image, but after that it does distant transformations much faster than this is done for commonly used inner-distances, so with a mass query, the gain in time consumption is powerful. A computational experiments demonstrate that the proposed method of specifying distances is more resistant to a fairly wide class of flexible articulations than the usual geodesic distance and, especially, Euclidean one. The way to develop our approach is to design a more efficient procedure for comparing descriptors.

ACKNOWLEDGEMENTS

The work was funded by Russian Foundation of Basic Research grant No. 20-01-00664.

REFERENCES

- Belongie, S. J., Malik, J., and Puzicha, J. (2002). Shape matching and object recognition using shape contexts. *IEEE Transactions on Pattern Analysis and Machine Intelligence*, 24(4):509–522.
- Boluk, S. A. and Demirci, M. F. (2015). Shape classification based on skeleton-branch distances. In *Proceedings of the International conference on computer vision theory and applications (VISAPP 2015)*, pages 353–359. SCITEPRESS, Portugal.
- Bronstein, A. M., Bronstein, M. M., Bruckstein, A. M., and Kimmel, R. (2008). Analysis of two-dimensional non-rigid shapes. *International Journal of Computer Vision*, 78(1):67–88.
- Cárdenes, R., Alberola-López, C., and Ruiz-Alzola, J. (2010). Fast and accurate geodesic distance transform by ordered propagation. *Image and Vision Computing*, 28(3):307–316.
- Cárdenes, R., Warfield, S. K., Macías, E. M., and Ruiz-Alzola, J. (2003). Occlusion points propagation geodesic distance transformation. In *Proceedings of the International Conference on Image Processing, ICIP 2003*, pages 361–364. IEEE.
- Cuisenaire, O. (1999). *Distance transformations: fast algorithms and applications to medical image processing*. PhD thesis, Université Catholique de Louvain, Louvain-la-Neuve, Belgium.
- Jain, V. and Zhang, H. (2005). Robust 2D shape correspondence using geodesic shape context. In *Proceedings of Pacific Graphics*, pages 121–124.
- Johnson, D. B. (1977). Efficient algorithms for shortest paths in sparse networks. *J. ACM*, 24(1):1–13.
- Ling, H. and Jacobs, D. W. (2007). Shape classification using the inner-distance. *IEEE Transactions on Pattern Analysis and Machine Intelligence*, 29(2):286–299.
- Lomov, N. and Mestetskiy, L. (2017). Pattern width description through disk cover – application to digital font recognition. In *Proceedings of the 12th International Joint Conference on Computer Vision, Imaging and Computer Graphics Theory and Applications (VISIGRAPP 2017), Volume 4: VISAPP*, pages 484–492. SCITEPRESS, Portugal.
- Mestetskiy, L. (2015). Medial width of polygonal and circular figures — approach via line segment voronoi diagram. In *Proceedings of the International conference on computer vision theory and applications (VISAPP 2015)*, pages 379–386. SCITEPRESS, Portugal.
- Mestetskiy, L. and Semenov, A. (2008). Binary image skeleton — continuous approach. In *VISAPP 2008 — 3rd International Conference on Computer Vision Theory and Applications, Proceedings*, volume 1, pages 251–258. SCITEPRESS — Science and Technology Publications, Portugal.
- Sethian, J. A. (1999). Fast marching methods. *SIAM Review*, 41(2):199–235.
- Shamai, G. and Kimmel, R. (2017). Geodesic distance descriptors. In *Proceedings of the Conference on Computer Vision and Pattern Recognition (CVPR 2017)*, pages 3624–3632. IEEE Computer Society.